SUPPLEMENTARY MATERIAL

Effect of calcium ions and pH on the morphology and mechanical properties of hyaluronan brushes

Xinyue Chen and Ralf P. Richter*

* *Corresponding author: email: r.richter@leeds.ac.uk*

TABLE OF CONTENTS

SUPPLEMENTARY METHODS

Refinement of the colloidal probe RICM analysis for coated glass substrates

In previous work,[1] we found an algorithm that is based on the quantification of the radial position of intensity extrema in colloidal probe interferographs[1,2] to work well for quantifying the thickness of HA brushes formed on bare glass. In the present work, HA brushes were formed on glass that was coated with a thin metal film. In the following, we show that the established method can also be applied on metal-coated glass with a simple modification.

We follow textbook knowledge[3] to describe the interference of light following transmission and reflection at multiple interfaces (Fig. S1*A*). For two parallel interfaces – formed by medium 0, an interlayer of medium 1, and medium 2 – the total reflectance *R*, which determines the reflected intensity $I_{\text{reflection}}$ for a given intensity $I_{\text{incidence}}$ of the incident light, is given by

$$R = I_{\text{reflection}} / I_{\text{incidence}} = |r_{012}|^2, \quad \text{(Eq. 1)}$$

where r_{012} presents the total effective reflection coefficient. This coefficient takes all light beams reflected back into medium 0 into account (Fig. S1*A*) and is given by

$$\begin{aligned} r_{012} &= r_{01} + t_{01}t_{10}r_{12}e^{-i2\beta} + t_{01}t_{10}r_{10}r_{12}e^{-i4\beta} + t_{01}t_{10}r_{10}{}^2r_{12}e^{-i6\beta} + \cdots, \\ &= r_{01} + [r_{01} + r_{12}\exp(-i2\beta)]/[1 + r_{01}r_{12}\exp(-i2\beta)] \end{aligned} \quad \text{(Eq. 2)}$$

where r_{xy} and t_{xy} are the local reflection and transmission coefficients at the interface between media *x* and *y*. The phase variation between two contiguous outcoming beams is constant. Assuming to a first approximation that light is incident perpendicular to the substrate, it is expressed as

$$\beta = 2\pi\tilde{n}_1 d / \lambda, \quad \text{(Eq. 3)}$$

where $\tilde{n}_1$ and *d* are the complex refractive index and the thickness of the interlayer, and λ is the wavelength of the incident light. Both reflection and transmission coefficients are then easily determined as

$$r_{xy} = (\tilde{n}_x - \tilde{n}_y)/(\tilde{n}_x + \tilde{n}_y) \text{ and } t_{xy} = 1 - r_{xy}. \quad \text{(Eq. 4)}$$

The complex refractive index, expressed as

$$\tilde{n} = n - i \cdot 2\pi k / \lambda, \quad \text{(Eq. 5)}$$

considers the refractive index *n* and the extinction coefficient *k*, and thus is appropriate for fully transparent layers (such as glass or the solution) as well as light-absorbing layers (such as Au).

The case of two interlayers can be reduced to the case of one interlayer (Fig. S1*B*), that is, the effective reflection coefficient r_{123} of a system consisting of media 1, 2 and 3 can first be determined by the approach described above, and then integrated with medium 0 by treating the two interlayers (made of media 1 and 2) as a single layer with effective optical properties. The total effective reflection coefficient is then

$$r_{0123} = r_{01} + [r_{01} + r_{123}\exp(-i2\beta)]/[1 + r_{01}r_{123}\exp(-i2\beta)]. \quad \text{(Eq. 6)}$$

This method can be further expanded for more interlayers.

To reproduce our experimental setup, we simulated the reflectance of a system consisting of a glass substrate, followed by a metal film (0.5 nm Ti adhesion layer + 5 nm Au), a hydrated organic film (8 nm, representing the OEG and SAv monolayers), a buffer layer of variable thickness (representing the space between the planar coated substrate and a given position on the surface of the colloidal probe; due to its strong hydration, the refractive index of the HA film can be considered equivalent to that of buffer to a good approximation) and a polystyrene medium (representing the colloidal probe). The optical properties used for the different media are provided in Table S1 and the results are shown in Fig. S1*C*.

The data in Fig. S1*C* illustrate the periodic dependence of the reflectivity on the probe-substrate distance. Importantly, the sinusoidal shape of the curve is not appreciably distorted by the metal film, alone (*red curve*) or in conjunction with the organic film (*blue curve)*, as compared to the bare glass (*black curve*), and the length of the period (λ / 2 n_{buffer}) also remains unchanged. The position of the extrema, on the other hand, is sensibly affected.

Table S1. Refractive indices and extinction coefficients used in the simulation of reflectance.

	Glass	Ti	Au	Organic film	Buffer	Polystyrene
n	1.514	1.771	1.017	1.450	1.333	1.550
k	0	2.374	1.826	0	0	0

These theoretical predictions justify our approach to analyze the experimental RICM data. Specifically, we used the analysis approach previously established for bare glass[1] to determine (i) the effective probe-surface distance H_{ref} on a reference surface featuring the metal film, the OEG monolayer and the SAv monolayer, and (ii) the effective probe-surface distance H_{HA} on an identically prepared surface with grafted HA. The real probe-substrate distance was then obtained as $H = H_{HA} - H_{ref}$. The offset by H_{ref} fully accounts for the effect of the metal and organic films on the position of the extrema with respect to the probe-surface separation.

We note in passing that Fig. S1*C* also shows that the maximal reflectance is enhanced with the metal film. This was indeed observed in the experiment and is an advantage as it enhances image contrast.

SUPPLEMENTARY FIGURES

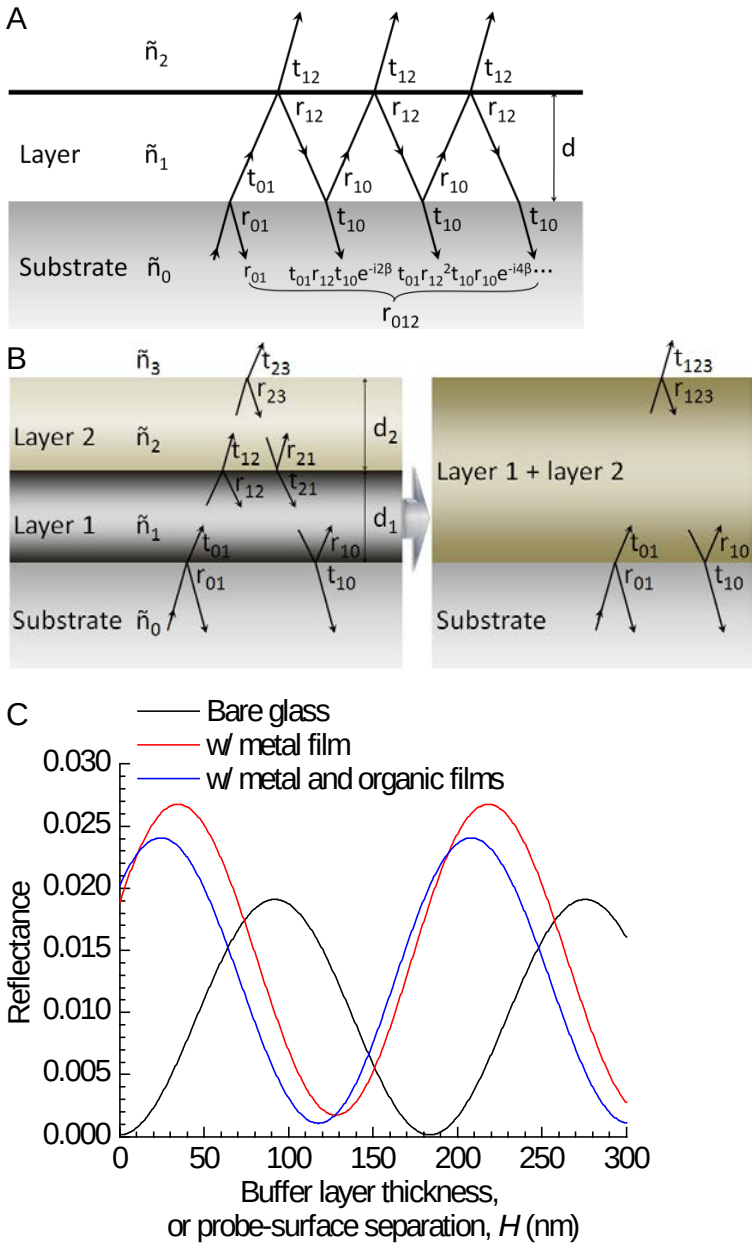

Figure S1. Impact of coatings on the glass substrate on RICM data analysis. (*A*) Schematic of the multiple reflections occurring at a single layer (medium 1) sandwiched between two other media (0 and 2). (*B*) Schematic of the light paths in a system with two layers and simplification to a single effective layer. (*C*) Simulated reflectance for a multilayer system consisting of a glass substrate, a buffer interlayer and polystyrene as a function of the buffer interlayer thickness *H* (for details see the text above and Table S1; λ= 490 nm). The glass was either bare (*black curve*), coated with a metal film (*red curve*), or coated with a metal film and an organic film (*blue curve*). In the experiment, the data would correspond to the reflectance at the centre of the colloidal probe as a function of the probe-surface separation *H*.

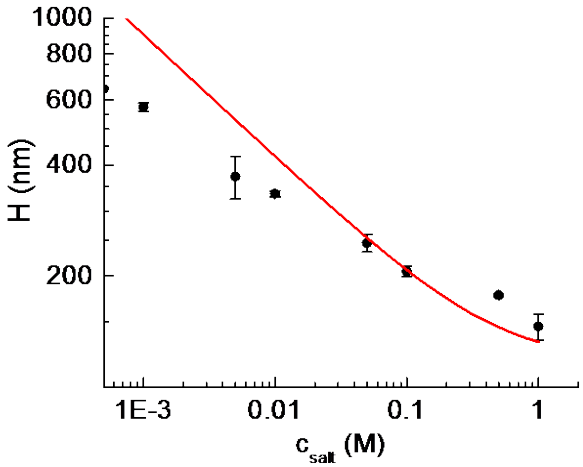

Figure S2. Estimation of grafting density. Unperturbed HA brush thickness measured at different NaCl concentration (*symbols*, extracted from Fig. 2) together with a fit (*line*, to data ≥ 50 mM NaCl) with a previously developed mean field theory.[4] From the fit, a root-mean-square distance s = 51 nm between anchor points is estimated.

The mean field approach treats HA as a semi-flexible polymer and the electrostatic repulsion between polyelectrolyte chains in the brush as an effective excluded volume, and has previously been found to describe HA brushes in NaCl solutions of sufficiently high ionic strength (≥ 50 mM) well.[4] Specifically, the thickness is predicted to depend on ionic strength as $H = (8/\pi^2)^{1/3} (pv/bs^2)^{1/3} l_c$, where l_c is the polymer contour length, b the monomer unit length, p characterizes the intrinsic chain stiffness, and v is the effective excluded volume. At high ionic strength, $v = v_0 + \alpha^2 / (4c_{NaCl})$, where α is the fractional charge per monomer unit and $v_0 = Ab^3$ the 'bare' excluded volume in the absence of charge repulsion (A is a numerical pre-factor, and depends on the monomer shape and the solvent quality). For the fitting, we used p = 14, b = 1 nm, A = 0.9 and α = 1 (as established in ref. 4), l_c = 740 nm (equivalent to 280 kDa HA), and s was the only adjustable parameter.

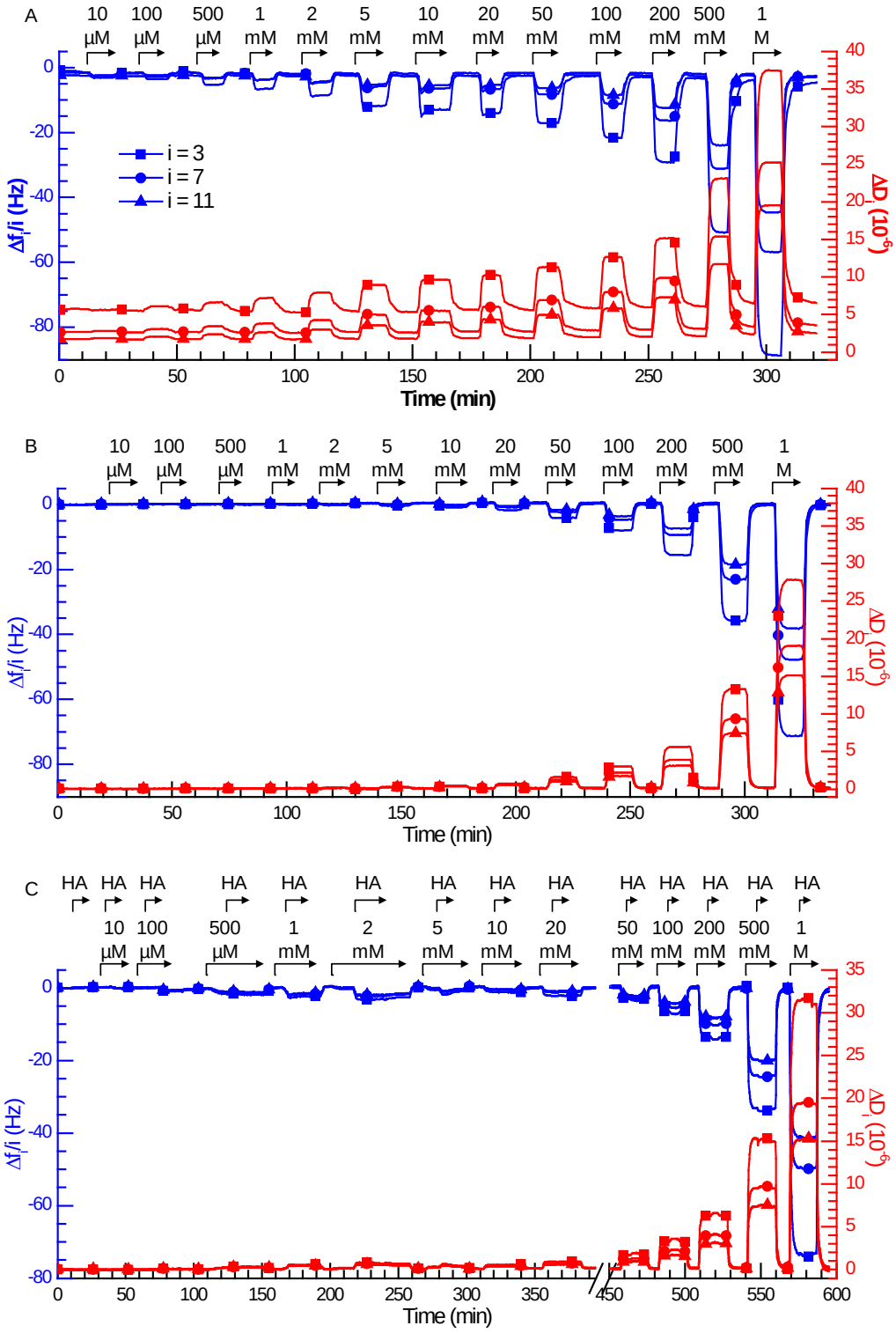

Figure S3. Effect of calcium ions on HA brushes, characterized by QCM-D. Representative time-resolved data for an HA brush (prepared as in Fig. 1*B*; *A*), a reference surface (SAv monolayer without HA; *B*), and non-specific binding of non-biotinylated HA to the reference surface (*C*). Shifts in normalized frequency, $\Delta f_i/i$, and in dissipation, ΔD_i, relative to a SAv monolayer in ultrapure water are displayed for overtones i = 3, 7 and 11 (as indicated in *A*). The start and duration of incubation of $CaCl_2$ (at various concentrations, as displayed) or HA (at 10 µg/mL) are indicated by arrows on top; during remaining times, surfaces were exposed to ultrapure water. The QCM-D responses upon incubation of $CaCl_2$ solution in *B* do not reflect any changes on the surface but result from changes in viscosity and/or density of the solution owing to the added $CaCl_2$. The frequency and dissipation shifts displayed in Fig. 3*A*-*B* were obtained by subtracting data in *B* from *A*, and essentially reflect the HA film alone.

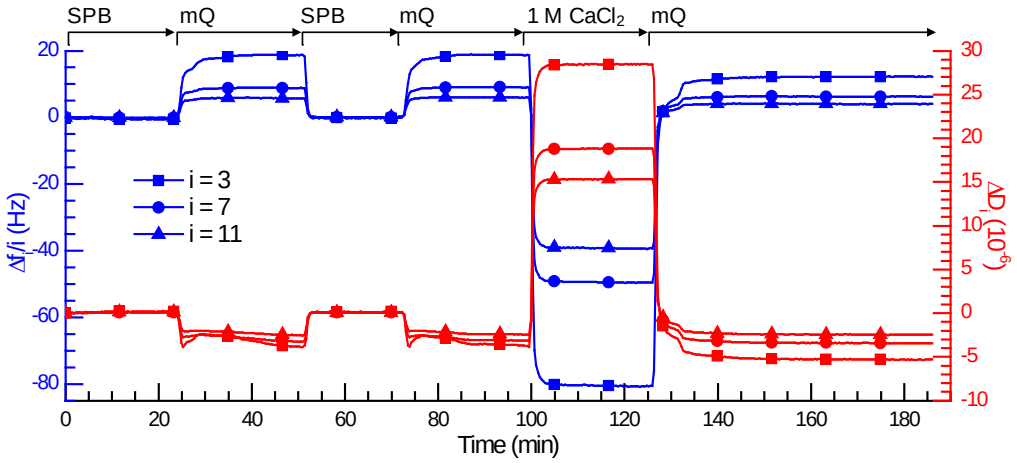

Figure S4. Reversibility of calcium effect on HA brushes. An HA brush was prepared as in Fig. 1*B*, and time-resolved QCM-D data at overtones i = 3, 7 and 11 for the response to various solutions (indicated by arrows on top) are shown. The transition from sample preparation buffer (SPB) to ultrapure water (mQ) is fully reversible, but 1 M $CaCl_2$ in ultrapure water has a minor irreversible effect on the HA brush.

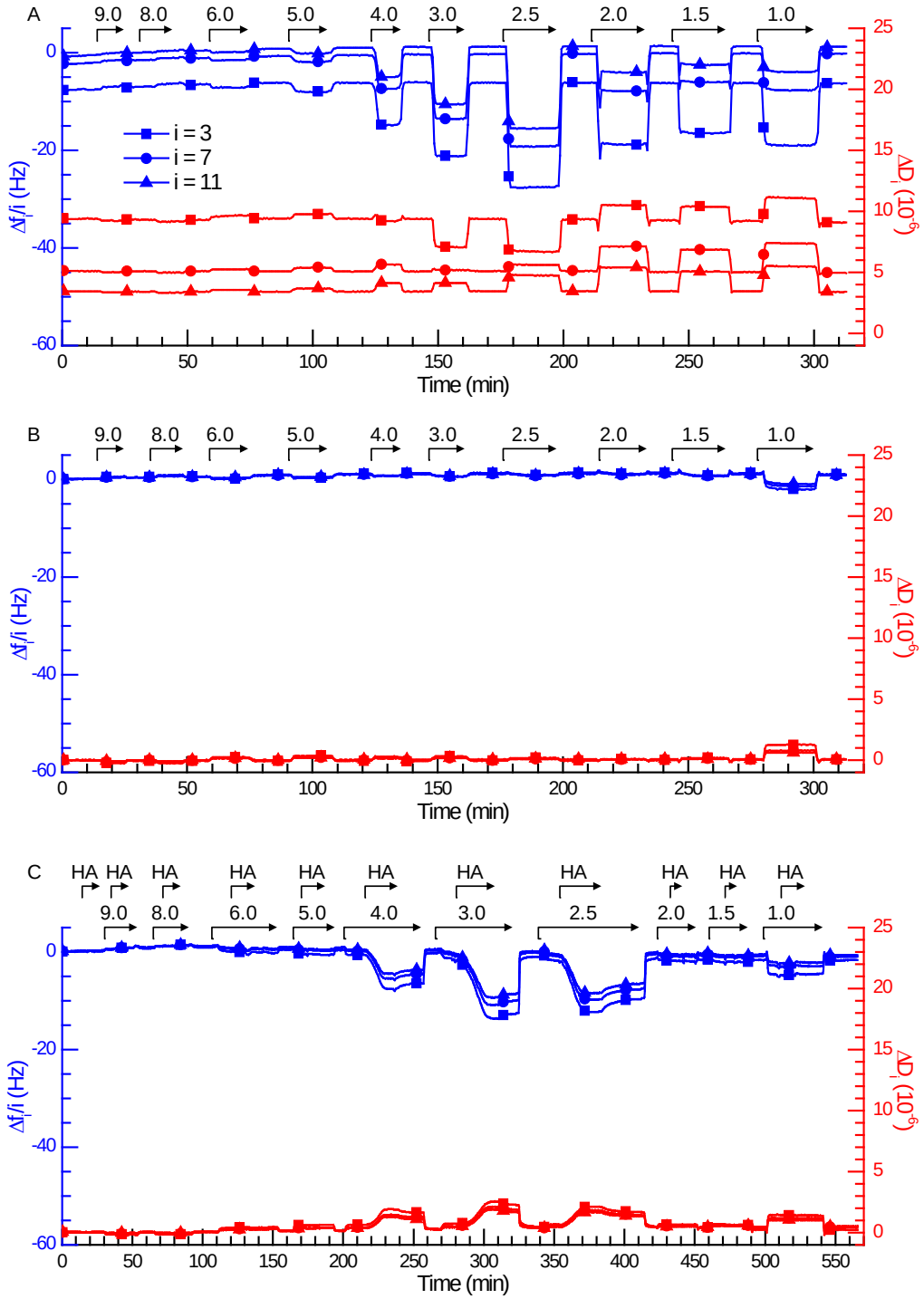

Figure S5. Effect of pH on HA brushes, characterized by QCM-D. Representative time-resolved data for an HA brush (prepared as in Fig. 1*B*; *A*), a reference surface (SAv monolayer without HA; *B*), and non-specific binding of non-biotinylated HA to the reference surface (*C*). Overtones i = 3, 7 and 11 are shown, as indicated in *A*. The start and duration of incubation of potassium phosphate buffer (containing 100 mM potassium ions at various pH, as displayed) or HA (at 10 µg/mL) are indicated by arrows on top; during remaining times, surfaces were exposed to potassium phosphate buffer at pH 7.0. The QCM-D responses upon incubation of solutions with different pH in *B* do not reflect any changes on the surface but result from changes in viscosity and/or density of the solution owing to the presence of added salt. The frequency and dissipation shifts displayed in Fig. 5*A*-*B* were obtained by subtracting data in *B* from *A*, and essentially reflect the HA film alone.

SUPPLEMENTARY REFERENCES

1. Attili, S.; Richter, R. P. Combining colloidal probe atomic force and reflection interference contrast microscopy to study the compressive mechanics of hyaluronan brushes. *Langmuir* **2012,** *28*, 3206-16.
2. Limozin, L.; Sengupta, K. Quantitative reflection interference contrast microscopy (RICM) in soft matter and cell adhesion. *ChemPhysChem* **2009,** *10*, 2752-68.
3. Fujiwara, H. Principles of optics. In *Spectroscopic Ellipsometry*; John Wiley & Sons, Ltd, 2007, pp 13-48.
4. Attili, S.; Borisov, O. V.; Richter, R. P. Films of end-grafted hyaluronan are a prototype of a brush of a strongly charged, semiflexible polyelectrolyte with intrinsic excluded volume. *Biomacromolecules* **2012,** *13*, 1466-77.